Proton radiotherapy offers immune-sparing benefits in glioblastoma treatment Proton therapy reduced radiation-induced lymphopenia

Julie Coupey, Thao-Nguyen Pham, Jérôme Toutain, Viktoriia Ivanova, Erika Hue, Charly Hélaine, Ali Ismail, Romaric Saulnier, Gaël Simonin, Marc Rousseau, et al.

Journal Pre-proof

Proton radiotherapy offers immune-sparing benefits in glioblastoma treatment Proton therapy reduced radiation-induced lymphopenia

J. Coupey , T.N. Pham , J. Toutain , V. Ivanova , E.S. Hue , C. Helaine , A. Ismail , R. Saulnier , G. Simonin , M. Rousseau , C. Moignier , J. Thariat , S. Valable

PII: S0360-3016(26)00010-6
DOI: https://doi.org/10.1016/j.ijrobp.2025.12.051
Reference: ROB 29888

To appear in: *International Journal of Radiation Oncology, Biology, Physics*

Received date: 15 July 2025
Revised date: 11 November 2025
Accepted date: 25 December 2025

Please cite this article as: J. Coupey , T.N. Pham , J. Toutain , V. Ivanova , E.S. Hue , C. Helaine , A. Ismail , R. Saulnier , G. Simonin , M. Rousseau , C. Moignier , J. Thariat , S. Valable , Proton radiotherapy offers immune-sparing benefits in glioblastoma treatment Proton therapy reduced radiation-induced lymphopenia, *International Journal of Radiation Oncology, Biology, Physics* (2026), doi: https://doi.org/10.1016/j.ijrobp.2025.12.051

Proton radiotherapy offers immune-sparing benefits in glioblastoma treatment

Proton therapy reduced radiation-induced lymphopenia

J. Coupey[1], T.N. Pham[1,2], J. Toutain[1], V. Ivanova[1], E. S. Hue[3,4], C. Helaine[1], A. Ismail[1], R. Saulnier[5], G. Simonin[6], M. Rousseau[6], C. Moignier[7], J. Thariat[2,8] and S. Valable[1*].

[1]Université de Caen Normandie, CNRS, Normandie Université, ISTCT UMR 6030, GIP CYCERON, F-14000 CAEN, France.
[2]Laboratoire de Physique Corpusculaire, UMR 6534 IN2P3/ENSICAEN – Normandie Université, France.
[3]LABÉO, 14280 Saint-Contest, France.
[4]Normandie Université, UNICAEN BIOTARGEN, 14280 Saint-Contest, France.
[5]UAR 3408/US 50, UNICAEN-CNRS-INSERM-CEA, Cyceron, GIP CYCERON, 14074 Caen, France.
[6]Université de Strasbourg, CNRS, IPHC UMR 7178, Strasbourg, F-67000, France.
[7]Medical physics department, Centre François Baclesse, Caen, France.
[8]Department of Radiation Oncology, Centre François Baclesse, Caen, France.
[*]Corresponding author

Corresponding author
Dr Samuel VALABLE
Université de Caen Normandie, CNRS, Normandie Université, ISTCT UMR 6030, GIP CYCERON, F-14000 CAEN, France.
Phone number: +33 2 31 47 01 08.
E-mail address: samuel.valable@cnrs.fr

Author responsible for statistical analysis

Dr Julie COUPEY

coupey@cyceron.fr

Contributors

In vivo experiments and analyses: JC, TNP, JeT, VI, CH, RS, GS, MR, SV

Cytokine and chemokine assays analyses: VI, JC

Immunostaining analyses: AI, JC

Flow cytometry acquisitions supervision: EH, JC

Conceptualization: JC, JeT, SV

Methodology: JC, SV

Funding acquisition: SV

Writing – original draft: JC, SV

Conflict of interest statement

The authors declare no conflict of interest relevant to the present manuscript.

Data availability statement for this Work

All data associated with this study are present in the paper or the supplementary materials or available from the authors upon request.

Funding statement / Acknowledgements

This work was supported by the CNRS (Centre National de la Recherche Scientifique) through the 80|Prime program; the Région Normandie (00129360-22E04690); the Ligue contre le Cancer; the Programme PAUSE-ANR Ukraine (Fonds d'urgence UKRAINE – Collège de France et ANR-22-PAUK-0033-01/ANR-23-PAUK-9033-01); the French National Agency for Research 'Investissements d'Avenir' (n°ANR-10-EQPX1401). This work was partly performed on a facility of France Life Imaging network (grant ANR-11-INBS-0006).

Graphical abstract

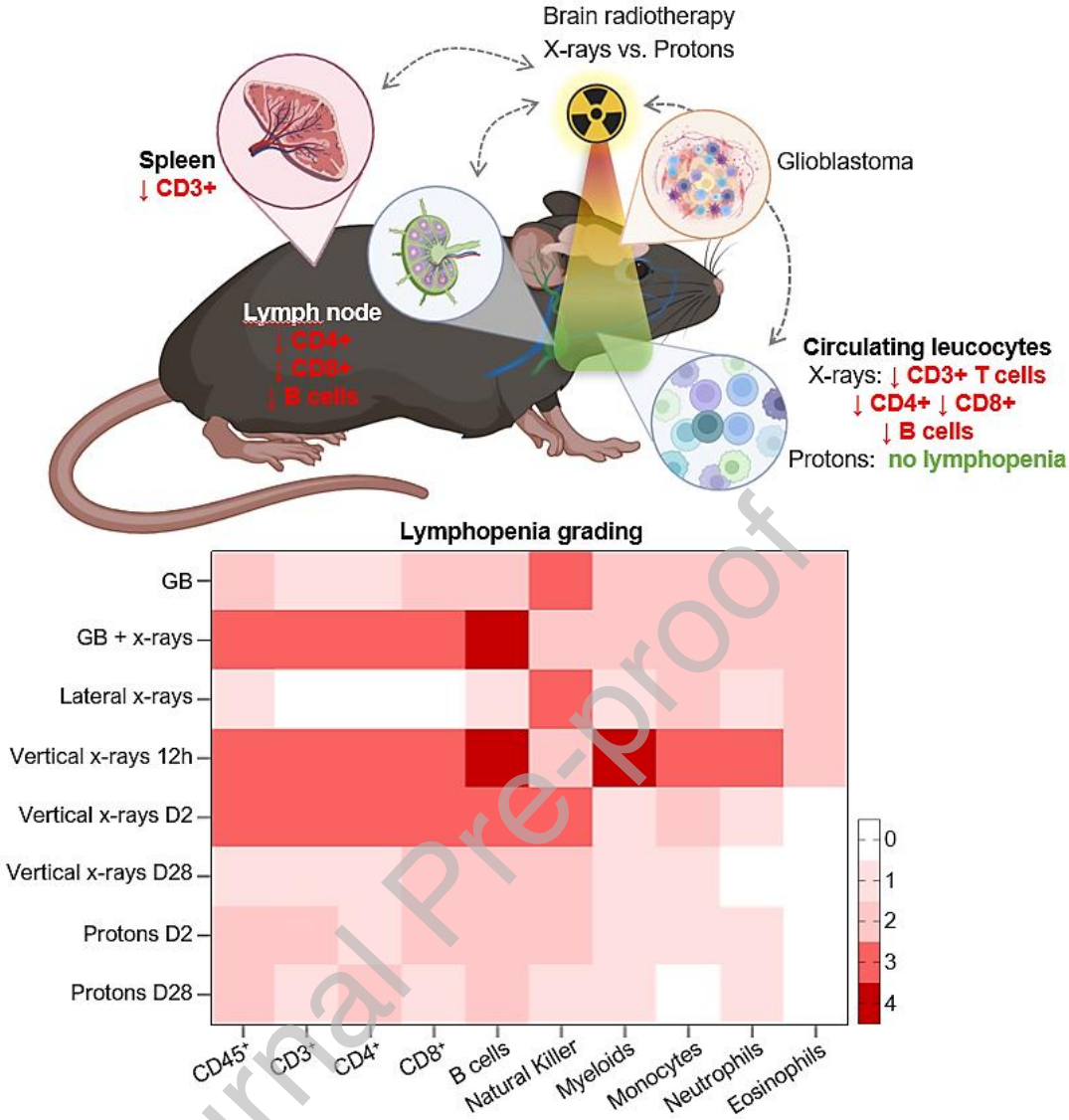

Abstract

Purpose

Glioblastoma (GB) and x-ray-based radiotherapy are associated with lymphopenia, which worsens prognosis and impairs anti-tumor immunity. Proton therapy, with its dosimetric properties that spare healthy brain tissue, is an alternative to reduce radiotoxicity. This study examined the effects of brain irradiation with x-rays or protons on lymphopenia.

Methods and Materials

We used GL261-tumor-bearing and tumor-free mice models to evaluate various lymphoid and myeloid cell populations after brain irradiation, assessing volume of brain irradiation, beam orientation, and lymphopenia onset timing via flow cytometry.

Results

In the GB mouse model, both tumor- and radiation-induced lymphopenia were evidenced. Severe lymphopenia, with a 50% depletion of $CD45^+CD3^+$ lymphocytes, $CD3^+CD4^+$ and $CD3^+CD8^+$ T cell, $CD3^-B220^+$ B cells, and $CD45^+CD11b^+$ myeloids, $CD11b^+Ly6C^+$ monocytes and $CD11b^+Ly6G^+$ neutrophils, occurred as early as 12 hours after x-ray exposure in tumor-free mice. Myeloid subtypes recovered by day 2, while lymphocyte recovery was cell-type dependent. The use of a lateral x-ray beam failed to alter circulating lymphocyte counts. Brain, cervical lymph nodes (CLN) and spleen immune cell quantification revealed a reduction in $CD3^+CD4^+$, $CD3^+CD8^+$ T and $CD3^-B220^+$ B cells post-x-ray exposure. Protons caused a 15% decrease in circulating lymphocytes, with no change in myeloid cells. Proton exposure also reduced $CD3^+CD4^+$ T and $CD3^-B220^+$ B cells in the CLNs but did not affect the spleen. Plasma cytokine levels in the IL-1 and MIP families correlated with leucocyte changes following exposure to both particle types.

Conclusions

We describe that proton therapy resulted in less lymphopenia than proton radiation, and propose that the mechanism may be related to biological processes rather than solely decreased exposure of circulating lymphocytes. This may be used to guide incorporation of immune therapy in GB.

Keywords: radiation-induced lymphopenia, x-ray radiotherapy, proton therapy, immunity, leucocytes, glioblastoma.

Synopsis

Understanding how brain irradiation affects circulating immunity can inform strategies to improve brain tumor treatment. This involves combining irradiation with immunotherapy and adjusting clinical protocols to restore lymphocytes/boost anti-tumor T cells.

Introduction

The immune system is composed of various cells commonly divided into lymphoid and myeloid lineages that ensure the immune response through synthesis and secretion of cytokines and chemokines[1]. Lymphocytes form phenotypically and functionally heterogeneous immune populations, including B and T lymphocytes (the latter are divided into cytotoxic $CD8^+$, conventional helper-auxiliary $CD4^+$ and regulatory (Treg)), as well as natural killer (NK) cells are involved in innate immunity[2]. Myeloid cells mainly comprise neutrophils and monocytes, which are phagocytic cells homing into tissues to differentiate into macrophages[3].

Beyond physiological functions, these cells play an essential role in the tumor microenvironment (TME)[4] and contribute to inflammation[5]. In the context of brain neoplasms, the TME is considered to be a multicompartmental system among which hypoxia, angiogenesis and the immune system are the main actors[6]. Immune cells have a central role in the control of tumor growth[7] and in treatment responses[8,9]. In specific conditions, such as high-grade gliomas, circulating immune cells count is low[10,11], which contribute to poor responses to immunotherapy[12]. Furthermore, the balance between the proportion of $CD4^+$ and $CD8^+$ lymphocytes is associated with a poor prognosis and tumor progression in glioblastoma (GB)[8]; this could also explain the difficulties in treating high-grade brain tumors with immunotherapy. In such conditions, the TME is considered as immunosuppressive[10]. Lymphopenia has also been frequently described in patients, and has been attributed to the tumor *per se*[13,14] or to its treatments[15].

Radiation-induced lymphopenia (RIL) has been reported after irradiation of several cancer types, including brain tumors[16,17]. T cells are indeed of the most radiosensitive immune cells, with a D10 (dose required for a 10% survival fraction) estimated at 3Gy[18,19]. Grossman *et al.* (2011) showed that for more than 10% of GB patients, the $CD4^+$ T cells count was below $200/mm^3$ ($500/mm^3$<baseline<$1500/mm^3$) at the end of chemo-radiotherapy[15]. In a *in silico* modelling irradiation study, Yovino *et al*. (2013) reported that after 30 fractions of radiotherapy, 99% of the blood pool received a dose greater than 0.5Gy[20]. Since, the literature demonstrated that RIL can persist for several months after irradiation associated with poor prognosis as well as accelerated tumor progression[21]. In addition, RIL's incidence and severity may depend on

volume of irradiation, fractionation, radiation type, and baseline lymphocyte count[22,23]. Conventional x-rays-mediated lymphopenia may explain, at least in part, the lack of the anti-tumor immune response in the treatment of high-grade brain tumors. Also, Ghosh *et al.* (2023) observed concomitantly a decrease of T cell count and an increase of myeloid-derived suppressors cell number in the blood of GB patients treated with chemoradiotherapy[17]. However, few studies are currently available that addressed the effects of brain irradiation on each lymphocyte and myeloid subtypes and the underlying mechanisms.

In order to circumvent the x-rays' side-effects, other radiotherapy modalities including proton therapy have emerged. Hammi *et al*. (2020), using a modeling study, demonstrated that the irradiated blood volume was smaller when protons were applied[22]. Similarly, in GB patients, proton therapy significantly reduced the irradiated volume that was associated to a lower RIL incidence[23]. These data suggest that proton therapy would likely be of interest to protect lymphocytes and preserve the anti-tumoral immune response. It could be mediated by changes in cells and tissues that are exposed to beam, that could, in turn and via the release of circulating factors, modulate RIL extent[24]. Little is known about the biological mechanisms underlying differential immune cell depletion after proton or photon irradiations. Also, the effects of x-rays/protons on the various leucocyte subpopulations needs to be further addressed.

Herein, we first explored the changes in the systemic immunity by measuring circulating lymphoid and myeloid subpopulation counts in a glioblastoma model after x-ray brain irradiation. To get rid of the tumor's effect, we then used tumor-free mice and challenged the irradiation volume (whole-brain or hemisphere), the beam orientation, the lymphopenia onset time and the type of radiotherapy particle (photons or protons). In parallel, cytokines, chemokines and brain cellular reactions were evaluated to get insights in the underlying mechanisms of RIL.

Methods

Ethics statement

This study was performed in accordance with the current European regulations, with permission of the regional committees on animal ethics.

Study design

First, in a glioblastoma C57BL/6 female mouse model (Janvier Labs laboratories, France), peripheral blood samples were collected during and after x-ray brain irradiation (n=5). Then, we assessed the impact of brain exposure to x-ray (n=20) or proton (n=20) on peripheral immunity in tumor-free mice. In parallel, in the same tumor-free model, the impact of beam orientation was evaluated.

Glioblastoma model

The murine glioblastoma cell line GL261 (Cellosaurus CVCL_Y003) (NCI-FREDERICK-DCTD, REPOSITORY) was used and cells were maintained in RPMI medium (*RO883*, Sigma-Aldrich) supplemented with 10% fetal calf serum (FCS, *CVFSVF00-01*, Eurobio Scientific), 1% glutamine (*G7513*, Sigma-Aldrich) and 1% penicillin/streptomycin (*P4333*, Sigma-Aldrich) at 37°C with 5% CO_2 and 95% air. Anesthetized (5% isoflurane for induction and 2% for maintenance in 70%N_2O/30%O_2) mice were placed on a stereotactic head holder. A 1mm diameter burr hole was drilled in the skull, 2mm left from the bregma. GL261 cells (1.10^5/3µL of 2mM Gln/PBS) were then injected at a depth of 4mm with a 30G needle flow of 0.6µL/min. Buprenorphine (*54000561*, Buprécare®, 0.05mg/kg) was administered in the perioperative phase.

X-ray irradiations

Vertical irradiations

X-ray irradiation sessions delivered a physical dose of 2.5Gy/fraction at 2Gy/min on anesthetized mice. Eight control (CTL) mice were also anesthetized but not irradiated. Mice were irradiated under anesthesia (5% isoflurane for induction and 2% for maintenance in 70%N_2O/30%O_2), twice daily for four consecutive days, up to a total dose of 20Gy. Two sub-groups were constituted: hemispheric (H) and whole-brain (WB) irradiation volume at 2Gy/min.

Treatment planning was performed using the SmARTPlan Treatment planning system software for small animal radiotherapy studies. X-ray irradiations were performed on the small animal irradiator XRad-225Cx (Cyceron platform, Caen, France) using an 8mm square collimator for whole-brain or left hemisphere irradiations after identification by the inboard scanner in order to spare the olfactory bulbs and the brainstem. After a scanner control with an aluminium filter (80 keV/0.5 mA) to set the beam, the treatment was applied using a copper filter (225 keV/13 mA).

Lateral irradiations

Our work showed that lymphopenia is at nadir under WB irradiation conditions and as early as 12 hours after irradiation. These conditions were applied to the lateral beam study. X-ray lateral irradiations delivered at unique physical dose of 5Gy (2*2.5Gy) at 2Gy/min in two lateral beams delivering 1.25Gy. Mice were irradiated under the same conditions as described above.

Protons irradiations

Proton irradiations were carried out at the PRECy platform (Strasbourg, France) on the CYRCé cyclotron (25MeV) using square or rectangular collimators enabling whole-brain or hemispheric irradiations and sparing the olfactory bulbs and the brainstem. The beam delivered a physical dose of 2.5Gy/fraction at 2Gy/min. As with x-rays, mice were irradiated under anesthesia (5% isoflurane for induction and 2% for maintenance in 70%N_2O/30%O_2), twice daily for four consecutive days, up to a total dose of 20Gy. Two sub-groups were constituted: hemispheric and whole-brain irradiation.

Flow cytometry

Blood samples

Peripheral whole blood samples were collected at different time points from mice after brain irradiation. For each mouse, 110µL of blood was collected from the submandibular vein using a sterile lancet (*GR-4MM*, Goldenrod animal lancet, BiosebLab) as described in the literature and as recommended in practice guidelines[25,26,27]. Blood samples (20µL) were transferred onto

96-wells V-bottom plates, treated twice with 1X red blood cell lysis buffer (*00433357*, ThermoFisher). The cell labeling protocol was performed as described in a previous study[28]. Multispectral flow cytometry was performed on a Cytoflex S® (Beckman Coulter, Flow cytometry accommodation, Normandie equine Vallee platform, LABEO BIOTARGEN, Saint-Contest, France) equipped with 405-, 488-, 561- and 638-nm lasers and 13 detectors for acquisition of fluorescence. Data were processed using the Kaluza® software (Beckman). A gating strategy was then developed to identify each blood (**Fig.S1**) immune cell subtypes[28]. The number of cells/µL was calculated and normalized by the number of recorded counting beads. The degree of lymphopenia was classified according to the Common Terminology Criteria for Adverse Events (CTCAE) version 5.0 as a percentage relative to CTL: 0.9 < grade 1 < 1; 0.6 < grade 2 < 0.89; 0.3 < grade 3 < 0.59; 0 < grade 4 < 0.29[14].

Lymph node samples

Cervical lymph nodes samples were thawed for 1 min at 37°C, then mechanically dissociated and passed through a 40mm diameter filter to recover only the cell suspension. The cell labeling protocol was performed as described above[28]. A gating strategy was developed to identify each immune cell subtypes (**Fig.S2**).

MR Imaging

Animals were anesthetized (2% of isoflurane in 70%N_2O/30%O_2), and brain magnetic resonance imaging (MRI) was performed at 7 Tesla (Bruker, Cyceron, Caen, France) at day 35 after brain irradiation. T2-weighted sequences were employed (RARE=8, TR/TE=5000/56msec, number of average=2, FOV=20*20mm, spatial resolution=0.078*0.078mm, 20 slices of 0.5mm thickness, and acquisition time=4min). Spleen volume was quantified by three people who were blind of the experimental group.

Immunohistochemistry

At D_{45}, mice were deeply anesthetized and transcardially perfused using a heparin/saline solution over 20 minutes after buprenorphine injection (0.05mg/kg). The brain and spleen were

removed and freezed in isopentane. 20µm thick cryostat brain sections were performed and stored at -80°C. Slices were rehydrated and blocked with PBS/0.1%Tween/0.5%Triton/3% BSA for 2h and incubated overnight with primary antibodies in PBS/0.1%Tween/0.5%Triton/1%BSA at 4°C. Sections were then incubated with fluorochrome-conjugated secondary antibodies and Hoechst 33342 (*14533*, Sigma-Aldrich) in PBS/0.1%Tween/0.5%Triton/1% BSA. Brain sections images were acquired with a microscope Leica DMi8, processed with the ImageJ software and then analyzed with QuPath version 0.3.0 for quantification[29]. Two regions of interest were used, striatum and hippocampus. Anti-GFAP antibody was chosen to assess the astrocyte activation as well as anti-CD68 and anti-Iba1 antibodies to evaluate the inflammatory tissue reaction through myeloid (CD68) and microglia (Iba1) activation. Quantification of GFAP labeling was performed as percentage area and absolute number of spots for CD68 and Iba1 inflammatory labeling.

Cytokine and Chemokine assays

Plasma was collected at each blood processing time point after a centrifugation step at 2000g for 10 minutes at 4°C and stored at -20°C for subsequent analyses. Detection and quantification of cytokines and chemokines were performed using BioLegend's LEGENDplex™ specific kits (*740446*/*740451*). Samples were run on the same Cytoflex S® (Beckman Coulter, Flow cytometry accommodation, Normandie equine Vallee platform, LABEO BIOTARGEN, Saint-Contest, France). Data were analyzed using BioLegend's LEGENDplex™ data analysis software. Data were expressed as the percentage changes relative to control.

Statistical analyses

Statistical analyses were performed using GraphPad Prism 10.4.1 (San Diego, CA). Data are presented as mean ± standard deviation (SD). The variation of immune cells compared with CTL and CD3 splenic staining were analyzed by a Kruskall-Wallis test. Tukey's test was used to analyze the changes in weight after brain irradiation. CD68/Iba1 brain immune staining was

analyzed by a two-way ANOVA along with a Fisher's LSD test, and GFAP brain staining was analyzed by a Kuskall-Wallis test. Variation in spleen volume was analyzed by a Holm-Sidàk's test. Statistical significance was declared if p <0.05, otherwise it was not significant.

Results

X-ray brain irradiation induces severe lymphopenia in GL261 tumor model.

We first explored the changes in circulating immune cells after x-rays brain irradiation in the context of brain tumor. We used the GL261 tumor bearing mice model which was submitted to brain irradiation (**Fig.1A**). As expected, the tumor grew over time as confirmed with MRI. Whole-brain radiotherapy with x-rays significantly reduced tumor growth (p<0.0001) (**Fig.1B**). The body weight, monitored as readout of the general status, of the control mice was stable, while only untreated tumor-bearing mice (GL1261) lost weight compared with CTL (**Fig.1C**).

We assessed the change in circulating $CD45^+$ leucocytes. At forty-eight hours (D_2) after irradiation (i.e., D_{12} after tumor cells implantation), data showed no significant change for the GL261-group compared to CTL, except a decrease in NK cells (p=0.0051). After x-ray brain irradiation, there was a significant decrease in $CD45^+$ (p=0.0003), $CD3^+$ (p=0.0023), $CD4^+$ (p=0.0397), $CD8^+$ (p=0.0003), B cells (p=0.0002) and NK (p=0.0051) in comparison to CTL (**Fig.1D**). No significant change was detected for both neutrophils, eosinophils, and monocytes in GL261- or GL261+x-rays groups compared with CTL (**Fig.1E**).

At D_7 following the irradiation (i.e., D_{19} of tumor growth), the results showed a significant reduction in leucocytes (p=0.0015), and all lymphocyte subtypes for the GL261-group compared with CTL (p=0.0025 for $CD3^+$; p=0.0250 for $CD4^+$; p=0.0009 for $CD8^+$; p=0.0030 for B cells; p=0.0007 for NK) (**Fig.1D**). The same holds true for x-ray-treated mice (p=0.0379 for $CD45^+$; p=0.0103 for $CD3^+$; p=0.0011 for $CD8^+$; p=0.0267 for B cells), except for $CD4^+$ and NK cells, which tended to recover at CTL level (**Fig.1D**). Also, no difference was shown at D_7 in myeloid subtypes compared with CTL (**Fig.1E**). Taken together, the data showed that the presence of the brain tumor alone induced a lymphopenia which was accelerated by x-ray irradiation.

X-ray brain irradiation alone induces an acute decrease in T cell subtypes in tumor-free mice.

To eliminate tumor effects and study only the action of radiotherapy on immune blood cells, we performed an irradiation protocol in tumor-free mice (**Fig.2A**). In this protocol, we introduced two distinct irradiation protocols: whole-brain (WB) and hemispheric (H) (**Fig.2B**) so as to assess lymphopenia and volume of irradiated brain. The body weight was not significantly changed after hemispheric irradiation. However, a significant weight loss was observed in the WB-irradiated group, reaching a maximum at 10 days after the irradiation (-2.7g, $p<0.0001$) (**Fig.2C**).

$CD45^+$ cells significantly reduced by approximately 50% after X-ray irradiation for the WB-irradiated group ($p=0.0125$) in comparison with CTL (**Fig.2D**). The $CD45^+$ count for the H-irradiated group was not significantly different in comparison to the CTL group (**Fig.2E**).

We then explored in details the lymphocyte and myeloid subpopulations. At D_2, there was a significant decrease in $CD3^+$, $CD4^+$, $CD8^+$, B and NK cells in response to x-rays. This effect was pronounced in WB-irradiated groups with $p=0.0005$ for $CD3^+$, $p=0.0317$ for $CD4^+$, and even more pronounced for $CD8^+$ cells in both irradiated groups ($p<0.0001$ for WB and $p=0.0138$ for H). The B cell population decreased by more than half compared with CTL after x-rays in both WB- ($p=0.0019$) and H-irradiated groups ($p=0.0039$). Similar observations were made for NK cells ($p=0.0067$ for H- and $p=0.0284$ for WB-irradiated groups) (**Fig.2E**).

Our next step consisted in evaluating the effect of x-rays brain exposure on myeloid cells, of which monocytes, neutrophils and eosinophils (**Fig.2F**). At D_2, there was no significant difference among irradiated groups and CTL (**Fig.2F**).

Taken together, the results showed a grade 3 x-ray-induced lymphopenia, affecting leucocytes and mostly $CD3^+$ subtypes, as well as B and NK cells. The difference in irradiation volume between WB and H did not lead to any change in the severity of RIL.

The temporal evolution of x-ray-induced lymphopenia is cell type dependent.

The recovery kinetics of lymphopenia was analyzed between D_2 and D_{28} for each lymphoid subpopulation. For $CD45^+$ leucocytes and all $CD3^+$ subtypes, as well as B and NK cells, the decrease at D_2 was followed by a recovery at D_{14} that went beyond the CTL level for hemispheric irradiation, and stabilized until D_{28}. This recovery is delayed for the WB-irradiation groups, as evidenced by the decrease observed at D_{14} for $CD3^+$, $CD8^+$, $CD4^+$. A similar pattern was observed for NK, which do not return to baseline levels by D_{28} ($p=0.0461$ for WB- and $p=0.0121$ for H-irradiation) (**Fig.S3**). Taken together, the data showed that the temporal progression of x-ray-induced lymphopenia depends on both the cell type and the irradiation volume.

Lymphopenia occurred as early as 12 hours after brain exposure to a vertical x-ray beam.

We next explored the timing of the onset of lymphopenia, the question being whether D_2 was the nadir of circulating lymphocyte pools or if a recovery already occurred (**Fig.3A**). Based on the data obtained from varying the irradiation volume, we chose to restrict our analysis to WB irradiation volume for the following studies. We focused on an even earlier time point: 12 hours after WB irradiation with the conventional vertical x-ray beam (corresponding to a dose of 5Gy). A significant decrease in $CD45^+$ ($p<0.0001$), $CD3^+$ ($p<0.0001$), $CD4^+$ ($p<0.0001$), $CD8^+$ ($p<0.0001$), and B cells ($p<0.0001$) compared with CTL was observed (**Fig.3B**). Data showed also a significant loss of myeloid cells ($p=0.0005$), monocytes ($p=0.0020$), and neutrophils ($p=0.0258$) compared with CTL (**Fig.3B**). Our findings indicated a grade 4 severe lymphopenia 12 hours following brain irradiation at 5Gy, involving nor only lymphocyte subpopulations but also myeloid cells.

Lymphopenia is delayed by the use of a lateral beam.

Since we observed significant changes in circulating leukocytes as early as 12 hours, after exposure to 5Gy using the vertical beam (**Fig.3**), we then applied the same protocol to the lateral beam. The vertical x-rays extend beyond the brain, also encompassing the lower part

of the head -notably the chin/neck, skull base nodes and large vessels feeding the brain (referred to as lymphocyte-rich organs (LRO))- which is consistent with previous simulation studies. To address if the effect was mediated by dose deposition in the brain but also in organs out of the brain, we used a lateral beam to assess the involvement of these region in the RIL (**Fig.3C**). The beams calculation and dose-volume histogram showed that LRO, including lymph nodes, received almost no dose with the two lateral beams as compared to the horizontal irradiation (**Fig.3C**). The dose to the brain was similar between horizonal and vertical beams, but not that received by LRO. The x-ray brain irradiation with a lateral beam did not induce significant change in all blood cell populations except an increase in $CD8^+$ ($p=0.0167$) (**Fig.3D**).

We also followed the evolution of lymphoid cells over time after the use of a lateral x-ray beam (**Fig.S4**). No change was measured at D_2 compared with CTL, except for a significant decrease in NK cells ($p=0.0063$) compared with CTL. At D_7, there was a significant decrease in $CD45^+$ ($p=0.0027$) and B cells ($p=0.0124$) (**Fig.S4**). Taken together, the data showed that the use of a lateral beam did not induce an acute lymphopenia compared to the vertical x-ray beam. However, lymphopenia was delayed and appeared at D_7 with no return to CTL levels for $CD8^+$ T cells and B cells. Taken together, our data demonstrated that sparing the CLNs suppressed the RIL phenomenon, although a delayed effect was observed in specific lymphocyte subsets.

Proton brain irradiation fails to change T cell subtypes nor in myeloid populations counts.

Based on the previous data comparing vertical and lateral irradiation and showing that irradiation of the LRO had a significant effect on RIL, we therefore evaluated the interest of a vertical proton irradiation instead of x-rays to spare circulating immune cells (**Fig.4A-B**). Proton brain exposure did not induce any variation in mice body weight compared with CTL (**Fig.4C**). Forty-eight hours after irradiation, no significant change occurred within the irradiated groups after proton exposure, irrespective of the irradiation volume for both lymphoid and myeloid cell subtypes (**Fig.4D-E**). We then assessed the recovery kinetics between D_2 and D_{28} for each

lymphoid subpopulation after proton irradiation (**Fig.S5**). Lymphocyte cell counts were stable early after proton exposure. Data showed a transient decrease in NK cells from D_2 to D_{14} with recovery to CTL level at D_{28} for both irradiation volume condition (**Fig.S5**).

The brain tissue inflammatory reaction is weaker after protons than after x-ray.

To understand if the difference observed for lymphopenia between x-rays and protons could be the results of a macroscopic tissue reaction, we performed brain MRI and to verify that cerebral exposure to x-rays and protons did not result in macro-anatomical changes or radionecrosis (**Fig.S6A**). To further assess the local inflammatory response after brain irradiation, we measured $CD68^+$ and $Iba1^+$ spots in the striatum and the hippocampus of both x-ray and proton protocols. In the striatum, a sustained increase of $CD68^+/Iba1^+$ labeling was observed after x-ray exposure compared to CTL ($p<0.0001$) (**Fig.S6B**). The quantification also confirmed that x-rays induced a more pronounced staining compared to protons ($p<0.0001$) (**Fig.S6B**). The hippocampus labeling revealed no significant difference between proton irradiation and the CTL group (**Fig.S6B**).

Star-shaped astrocytes were also clearly visible, with a more intense and diffuse labeling on irradiated slices compared with CTL (**Fig.S6C**). Following both x-ray and proton brain irradiation, activated astrocytes were prominently detected in irradiated brain regions, reflecting a sustained astrocytic response to radiation-induced tissue damage. Quantification confirmed that this astrocytic response was higher following x-rays compared with protons in both striatum ($p=0.0180$) and hippocampus ($p=0.0272$) areas (**Fig.S6C**).

Radiation-induced lymphopenia is mediated by lymphocyte damage in cervical lymph nodes and spleen.

Since LRO sparing in the lateral x-ray beam delayed and attenuated the radiation-induced lymphopenia and since proton also spared these LRO, and that our data revealed a local cerebral inflammatory reaction, we set out to find the link between cerebral irradiation and the drastic effect at blood level. Our first focus was on flow cytometry results on cervical lymph

nodes, which are present in the conventional x-ray beam field but not in the proton one. At D_2 where lymphopenia was severe, there was an increase in $CD4^+$ and $CD8^+$ subpopulations compared with CTL (**Fig.5A**). At D_{45} after x-rays, the results showed a significant decrease of more than half in $CD4^+$ ($p=0.0453$). The B cell population decreased almost completely compared to CTL ($p=0.0009$) (**Fig.5A**). After protons, a non-significant decrease was observed in $CD4^+$ T cells and B cells compared with CTL (**Fig.5A**).

To further explore the implication of LRO on peripheral immune cell variations, we measured the plasma levels of cytokines and chemokines in mice that were exposed to x-rays and protons. Analyses were performed at D_2, the time at which lymphopenia was compared for both type of irradiation. Data showed no significant difference in plasma of x-ray-irradiated mice compared with CTL, except for IL-1α for which expression level decreased compared with CTL. A decrease in chemokine expression level was detected for the MIP family, including MIP-3α and MIP-1α after x-rays compared with CTL (**Fig.5B**). Proton brain exposure induced an increase in IFN-γ and a decrease in IL-6 expression level. Chemokine assays showed a decrease CCL11, and MCP-1, and an increase in CXCL5 level expression (**Fig.5B**).

To further examine the impact of brain irradiation on the spleen, we studied the effects of x-ray and proton brain exposure on the splenic $CD3^+$ T cell population (**Fig.5C**). CD3 total labeling (in both red and white pulp) revealed a 50% reduction in CD3 fluorescence 12 hours after x-ray irradiation ($p=0.0253$) compared with CTL. Within the white pulp, there was a significant decrease in CD3 fluorescence 12 hours after x-rays ($p=0.0158$) but no difference 45 days after x-ray nor proton brain exposure compared with CTL. Within the red pulp, there was a significant decrease in CD3 fluorescence 12 hours ($p=0.0171$) after x-ray brain exposure, and 45 days (although not statistically significant) (**Fig.5C**).

Taken together, the data highlighted a functional involvement of LRO, particularly the CLNs and the spleen, in the development and maintenance of radiation-induced lymphopenia.

Discussion

In the context of brain tumors, our study demonstrated that mice with GB and subjected to x-rays exhibited significant lymphopenia detected on day 2 during the irradiation protocol (10Gy), which persisted over time (day 7), with no recovery to control levels. This finding is consistent with the study of Piotrowksi *et al.* (2018), whose results also demonstrate systemic lymphopenia following brain irradiation with x-rays, and with that of Ghosh *et al.* (2023)[17], although our data did not show an increase in myeloid cells. The significant reduction in circulating lymphocytes induced by x-rays could contribute to impairment of tumor-infiltrating T cells, which may explain the therapeutic challenges faced in studies the aim of which is the reactivation of immune cells against the tumor[30,31]. These findings highlight the potential for alternative radiotherapy approaches, such as proton therapy, which may be more well-suited with enhancing the immune response against the tumor. Therefore, the present study aimed to investigate RIL following brain irradiation with respect to the onset of lymphopenia, and beam orientation. Additionally, the impact of different radiotherapy particles (photons vs protons) on lymphocyte and myeloid subpopulations after brain irradiation was explored, to discern whether these effects were attributable to beam ballistics, cellular biology, or both factors.

Our results confirmed a significant acute reduction in circulating lymphocytes on day 2 after 10Gy following vertical brain x-ray exposure. These findings are consistent with those reported in the literature[15,20]. In an original manner, our investigations revealed a decrease in $CD3^+$, $CD4^+$, $CD8^+$, B, and NK cells as early as 12 hours post-irradiation, a level of detail not previously reported in the literature. Furthermore, we showed that $CD8^+$, B, and NK cells were more radiosensitive that $CD4^+$ cells.

No differences were observed in the myeloid subpopulations. However, changes within immunosuppressive subsets -such as anti-inflammatory TAMs and regulatory T cells- could be of particular importance, as they may also vary in response to irradiation-induced inflammatory effects in the brain and the blood[49]. Mitigating or counteracting RIL requires a

better understanding of how these immunosuppressive populations are altered following radiation exposure, as previously reported in the literature[50,51].

Lymphocyte radiosensitivity is well-documented[19], with a D10 of 3Gy[18]. In our experimental procedure, this dose was reached and event exceeded on the first day of the irradiation protocol (5Gy) in the brain tissues. Notably, this dose corresponds to the data obtained 12 hours after x-ray exposure, highlighting the rapid and acute onset of lymphopenia. Moreover, the extent of lymphopenia was independent of the irradiation volume, with recovery being delayed for whole-brain exposure compared to x-ray exposure restricted to one brain hemisphere. These results suggest that circulating leucocytes in the head likely received a significant dose during the irradiation process.

A caution should be taken as our murine model showed recovery of lymphocyte pools after irradiation, confirming data from the literature[48]; however, data in patients[15] demonstrated severe RIL that persists over time.

Based on biological theories in combination with mathematical modeling, we recently provided quantitative estimates of lymphocyte migration and residence times that indicated 2 hours in the spleen, 10 hours in lymph nodes, and less than 1 minute in the lungs and liver[19]. Only 5% of lymphocytes were present in the circulating blood compartment at all times. Our kinetics simulation in blood revealed that recovery from sudden lymphopenia (to more than 80% of their initial level) occurred in less than 200 minutes. These data are inconsistent with the hypothesis suggesting that leucocytes are directly irradiated by the beam. It is also reinforced by the results of our present study between whole-brain and hemisphere.

To further understand the mechanisms underlying RIL, we analyzed the relationships between brain and vascular dose maps and leukocyte subpopulations to construct a model estimating the radiation dose received by the blood, based on our preclinical experimental data[16]. Simulations showed that the dose delivered to the blood is low, with the maximum blood dose not exceeding 0.8Gy, regardless of the type of irradiation. The volume of blood exposed during brain irradiation is limited, representing approximately 1% of the total blood volume. This

proportion does not differ significantly between x-ray and proton irradiation[16]. RIL could therefore result from a combination of direct radiation-induced lymphocyte death and depletion of lymphocyte reserves in lymphoid organs following repeated fractionated irradiation protocols.

One can assume that lymphocyte counts within the irradiated area is twice greater in whole-brain than hemisphere but the lymphopenia was observed in both cases. However, this may explain the sudden onset of lymphopenia as early as 12 hours, and its absence in lateral beam irradiation condition. Indeed, conventional superior-inferior x-ray beam delivered radiation dose to the skull base nodes. On the contrary, the beams calculation and dose volume histograms showed that lymph nodes and large arteries received almost no dose using lateral beam. The severity and timing of RIL are therefore associated with beam orientation and, consequently, with the dose received by LRO present in the beam field. Interestingly, our data showed that lymphopenia occurred following the use of a lateral beam, but it was delayed than that observed after exposure to conventional vertical irradiation.

The change in the type of radiotherapy particle corroborated the data reported in the literature. The sparing effect of protons is consistent with findings from clinical studies[23], which may be attributed to the preservation of lymph nodes located below the brain. These results support the ballistic hypothesis. In addition to changes in blood parameters, a significant decrease in body weight was observed in x-ray irradiated mice, which could be linked to dose deposition in the salivary glands and masticatory muscles. During RT for head and neck cancers, the salivary glands are often unintentionally co-irradiated, leading to hyposalivation and xerostomia, which can severely affect the quality of life of patients[32]. Proton irradiation, combined with the use of a lateral beam, spared the LRO, explaining the absence of weight loss and lymphopenia. Given that lateral x-ray beams induced a delayed onset of lymphopenia compared to conventional vertical beams, the use of protons in cerebral irradiation appears highly beneficial for the treatment of solid brain tumors like GB.

Immunohistochemistry analyses revealed a brain tissue response, reflecting an activation of macrophages, microglia and astrocytes. Suckert *et al*. (2020) demonstrated that gliosis and astrocytic reaction occurred within the proton irradiation field, albeit at higher doses (>40Gy) than those used in our study[33]. In contrast, our findings indicate that proton irradiation specifically promoted local astrocyte activation, without any observed staining for CD68 and Iba1. These discrepancies between the two irradiation modalities may explain the observed variations in leucocytes responses, suggesting a preferential biological interaction between the brain and the blood.

Chongsathidkiet *et al*. (2018) demonstrated that lymphocytes were sequestered in the bone marrow of treatment-naïve GB patients and GB mouse models, with a concomitant splenic contraction in patients (mean size reduction of 32%), leading to lymphopenia[13]. Our data align with these findings, suggesting that T cells are sequestered in the cervical lymph nodes, thus explaining the reduction in splenic $CD3^+$ counts observed at 24 hours post-x-ray irradiation. Consequently, the observed decrease in $CD3^+$ counts in the spleen is consistent with lymphopenia following x-ray brain irradiation. These findings support the hypothesis of soluble factors released from irradiated cerebral tissues can be transmitted the bloodstream to peripheral hematopoietic organs[34,35]. Piotrowski *et al.* (2018) also reported that brain irradiation-induced lymphopenia was accompanied by severe structural changes in non-irradiated lymph nodes and spleen. To go further, compensatory changes in IL-7 levels suggest that this cytokine may play an important role in regulating lymphocyte recovery following RIL.

Taken together, the results point to a tangible biological mechanism for lymphopenia. The reduction in lymphocyte blood level would induce a compensation in the CLNs that would allow the blood recovery observed from D_8 or D_{14} after x-rays, inducing the depletion of T lymphocyte subtype stocks in lymph nodes at D_{45}. The study of Paganetti *et al.* (2023) concluded that radiation-induced lymphocyte death alone is unlikely to explain radiation-induced

lymphopenia[36]. Cytokine analysis of irradiated mouse plasma did not reveal changes that could explain early lymphopenia or differences between x-ray and proton beams.

A limitation of our study was the use of a healthy mouse model without inflammation or tumors. Future plasma analyses from tumor-bearing mice may clarify cytokine variations and mechanisms using more sensitive technologies[37,38]. While reduced expression of chemoattractant chemokines could obscure pro-inflammatory cytokine detection[39], it does not explain systemic lymphopenia or the differences between irradiation types. Previous studies suggest IL-1 upregulation in the acute phase after irradiation[40,41], coinciding with peak lymphopenia. Our data showed distinct inflammatory responses, with an association between levels of specific cytokines and variation in leucocyte subpopulations after brain exposure, which has been modeled and shown in a previous study: no correlation was detected at the individual level between the overall concentrations of $CD4^+$, $CD8^+$, B, or NK cells and cytokine levels. Only the naïve T cell population showed a significant association with cytokine levels. Variations in plasma cytokine levels also correlated with changes in neutrophils and monocytes[42].

A recent study demonstrated a nanostructure co-encapsulating a lymphopenia-alleviating agent and cytokine to enhance T-cell recruitment, suggesting promising therapeutic options[43]. These findings may influence strategies for immune modulation and highlight the potential for biomarkers to improve proton therapy[44].

Whether tumor-infiltrating lymphocytes, lymphocytes resident in the CLNs, or circulating blood lymphocytes, they are crucial for both cellular and humoral anti-tumor immunity. To preserve anti-tumor immunity and enhance the efficacy of immunotherapy, lymphocytes can be considered as an organ at risk in their own right[45]. Current efforts to optimize radiotherapy focus on minimizing exposure to circulating blood and LRO, in accordance with the ‘as low as reasonably achievable' (ALARA) principle[46]. It is therefore critical to assess when and how RIL mitigation strategies could benefit the treatment of solid brain tumors. Lymphocytes are vital components in the co-irradiation of normal tissues, presenting a challenge at the intersection

of radiotherapy and immunotherapy. The reprogramming of both systemic and local immune functions is essential for T-cell-based immunotherapy[47]. Proton therapy, which spares circulating immunity, offers a clinically translatable approach to improve brain tumor treatment and prognosis.

In conclusion, our work highlights two innovative avenues. First, lymphopenia develops rapidly across all lymphocyte subtypes following exposure to a vertical x-ray beam. Second, the use of advanced radiation therapy modalities that spare circulating lymphocytes should be considered to optimize treatment strategies. It could combine the reprogramming of local and systemic immune functions for T-cell based immunotherapy with proton therapy for patients undergoing brain irradiation.

Data sharing statement

All data associated with this study are present in the paper or the supplementary materials or available from the authors upon request.

List of abbreviations

CLN: cervical lymph nodes

CTCAE: common terminology criteria for adverse events

CTL: control

DVH: dose-volume histogram

GB: glioblastoma

GFAP: glial fibrillary acidic protein

Gy: gray

H: hemispheric

IFN: interferon

IL: interleukin

LRO: lymphocyte-rich organs

MDSC: myeloid-derived suppressor cells

MIP: macrophage inflammatory protein

NK: natural killer

PBS: phosphate buffered saline

TAM: tumor-associated macrophages

TME: tumor microenvironment

Treg: regulator T lymphocyte

RIL: radiation-induced lymphopenia

WB: whole-brain

References

1. Kansler ER, Li MO. Innate lymphocytes-lineage, localization and timing of differentiation. Cell Mol Immunol. 2019 Jul;16(7):627–33.

2. Parkin J, Cohen B. An overview of the immune system. The Lancet. 2001 Jun 2;357(9270):1777–89.

3. Geissmann F, Manz MG, Jung S, Sieweke MH, Merad M, Ley K. Development of monocytes, macrophages, and dendritic cells. Science. 2010 Feb 5;327(5966):656–61.

4. Sica A, Larghi P, Mancino A, Rubino L, Porta C, Totaro MG, et al. Macrophage polarization in tumour progression. Seminars in Cancer Biology. 2008 Oct 1;18(5):349–55.

5. Fecci P, Mitchell D, Whitesides J, Xie W, Friedman A, Archer G, et al. Increased Regulatory T-Cell Fraction Amidst a Diminished CD4 Compartment Explains Cellular Immune Defects in Patients with Malignant Glioma. Cancer research. 2006 Mar 1;66:3294–302.

6. Quail DF, Joyce JA. The Microenvironmental Landscape of Brain Tumors. Cancer Cell. 2017 Mar 13;31(3):326–41.

7. Hinshaw DC, Shevde LA. The Tumor Microenvironment Innately Modulates Cancer Progression. Cancer Res. 2019 Sep 15;79(18):4557–66.

8. Han S, Zhang C, Li Q, Dong J, Liu Y, Huang Y, et al. Tumour-infiltrating CD4(+) and CD8(+) lymphocytes as predictors of clinical outcome in glioma. Br J Cancer. 2014 May 13;110(10):2560–8.

9. Prosniak M, Harshyne LA, Andrews DW, Kenyon LC, Bedelbaeva K, Apanasovich TV, et al. Glioma grade is associated with the accumulation and activity of cells bearing M2 monocyte markers. Clin Cancer Res. 2013 Jul 15;19(14):3776–86.

10. Klemm F, Maas RR, Bowman RL, Kornete M, Soukup K, Nassiri S, et al. Interrogation of the Microenvironmental Landscape in Brain Tumors Reveals Disease-Specific Alterations of Immune Cells. Cell. 2020 Jun 25;181(7):1643-1660.e17.

11. Friebel E, Kapolou K, Unger S, Núñez NG, Utz S, Rushing EJ, et al. Single-Cell Mapping of Human Brain Cancer Reveals Tumor-Specific Instruction of Tissue-Invading Leukocytes. Cell. 2020 Jun 25;181(7):1626-1642.e20.

12. Tomaszewski W, Sanchez-Perez L, Gajewski TF, Sampson JH. Brain Tumor Microenvironment and Host State: Implications for Immunotherapy. Clin Cancer Res. 2019 Jul 15;25(14):4202–10.

13. Chongsathidkiet P, Jackson C, Koyama S, Loebel F, Cui X, Farber SH, et al. Sequestration of T cells in bone marrow in the setting of glioblastoma and other intracranial tumors. Nat Med. 2018 Sep;24(9):1459–68.

14. Kim WJ, Dho YS, Ock CY, Kim JW, Choi SH, Lee ST, et al. Clinical observation of lymphopenia in patients with newly diagnosed glioblastoma. J Neurooncol. 2019 Jun;143(2):321–8.

15. Grossman SA, Ye X, Lesser G, Sloan A, Carraway H, Desideri S, et al. Immunosuppression in patients with high-grade gliomas treated with radiation and temozolomide. Clin Cancer Res. 2011 Aug 15;17(16):5473–80.

16. XXXX et al. Int J Radiat Biol. 2024 Mar 11;1–12.

17. Ghosh S, Huang J, Inkman M, Zhang J, Thotala S, Tikhonova E, et al. Radiation-induced circulating myeloid-derived suppressor cells induce systemic lymphopenia after chemoradiotherapy in patients with glioblastoma. Sci Transl Med. 2023 Jan 25;15(680):eabn6758.

18. Nakamura N, Kusunoki Y, Akiyama M. Radiosensitivity of CD4 or CD8 positive human T-lymphocytes by an in vitro colony formation assay. Radiat Res. 1990 Aug;123(2):224–7.

19. XXXX et al. J Exp Clin Cancer Res. 2023 Feb 22;42(1):50.

20. Yovino S, Kleinberg L, Grossman SA, Narayanan M, Ford E. The etiology of treatment-related lymphopenia in patients with malignant gliomas: modeling radiation dose to circulating lymphocytes explains clinical observations and suggests methods of modifying the impact of radiation on immune cells. Cancer Invest. 2013 Feb;31(2):140–4.

21. Mendez JS, Govindan A, Leong J, Gao F, Huang J, Campian JL. Association between treatment-related lymphopenia and overall survival in elderly patients with newly diagnosed glioblastoma. J Neurooncol. 2016 Apr;127(2):329–35.

22. Hammi A, Paganetti H, Grassberger C. 4D blood flow model for dose calculation to circulating blood and lymphocytes. Phys Med Biol. 2020 02;65(5):055008.

23. Mohan R, Liu AY, Brown PD, Mahajan A, Dinh J, Chung C, et al. Proton Therapy Reduces the Likelihood of High-Grade Radiation-Induced Lymphopenia in Glioblastoma Patients: Phase II Randomized Study of Protons vs. Photons. Neuro Oncol. 2020 Aug 5;

24. Miszczyk J. Investigation of DNA Damage and Cell-Cycle Distribution in Human Peripheral Blood Lymphocytes under Exposure to High Doses of Proton Radiotherapy. Biology (Basel). 2021 Feb 3;10(2):111.

25. Golde WT, Gollobin P, Rodriguez LL. A rapid, simple, and humane method for submandibular bleeding of mice using a lancet. Lab Anim (NY). 2005 Oct;34(9):39–43.

26. Jo EJ, Bae E, Yoon JH, Kim JY, Han JS. Comparison of murine retroorbital plexus and facial vein blood collection to mitigate animal ethics issues. Lab Anim Res. 2021 May 6;37(1):12.

27. Francisco CC, Howarth GS, Whittaker AL. Effects on animal wellbeing and sample quality of 2 techniques for collecting blood from the facial vein of mice. J Am Assoc Lab Anim Sci. 2015 Jan;54(1):76–80.

28. XXXX et al. Methods Cell Biol. 2024;189:135–52.

29. Bankhead P, Loughrey MB, Fernández JA, Dombrowski Y, McArt DG, Dunne PD, et al. QuPath: Open source software for digital pathology image analysis. Sci Rep. 2017 Dec 4;7(1):16878.

30. Jarosz-Biej M, Smolarczyk R, Cichoń T, Kułach N. Tumor Microenvironment as A 'Game Changer' in Cancer Radiotherapy. Int J Mol Sci. 2019 Jun 29;20(13):3212.

31. Dapash M, Hou D, Castro B, Lee-Chang C, Lesniak MS. The Interplay between Glioblastoma and Its Microenvironment. Cells. 2021 Aug 31;10(9):2257.

32. Verhaegen F, Butterworth KT, Chalmers AJ, Coppes RP, de Ruysscher D, Dobiasch S, et al. Roadmap for Precision preclinical x-ray radiation studies. Phys Med Biol. 2022 Dec 30;

33. Suckert T, Beyreuther E, Müller J, Azadegan B, Meinhardt M, Raschke F, et al. Late Side Effects in Normal Mouse Brain Tissue After Proton Irradiation. Front Oncol. 2020;10:598360.

34. Mohye El-Din AA, Abdelrazzak AB, Ahmed MT, El-missiry MA. Radiation induced bystander effects in the spleen of cranially-irradiated rats. Br J Radiol. 2017 Dec;90(1080):20170278.

35. Koturbash I, Loree J, Kutanzi K, Koganow C, Pogribny I, Kovalchuk O. In vivo bystander effect: cranial X-irradiation leads to elevated DNA damage, altered cellular proliferation and apoptosis, and increased p53 levels in shielded spleen. Int J Radiat Oncol Biol Phys. 2008 Feb 1;70(2):554–62.

36. Paganetti H. A review on lymphocyte radiosensitivity and its impact on radiotherapy. Front Oncol [Internet]. 2023 Aug 3 [cited 2024 Sep 25];13.

37. Wang X, Yip KC, He A, Tang J, Liu S, Yan R, et al. Plasma Olink Proteomics Identifies CCL20 as a Novel Predictive and Diagnostic Inflammatory Marker for Preeclampsia. J Proteome Res. 2022 Dec 2;21(12):2998–3006.

38. Wang T, Yang S, Long Y, Li Y, Wang T, Hou Z. Olink proteomics analysis uncovers the landscape of inflammation-related proteins in patients with acute compartment syndrome. Front Immunol. 2023;14:1293826.

39. Noack M, Kolopp-Sarda MN. Cytokines et inflammation : physiologie, physiopathologie et utilisation thérapeutique. Revue Francophone des Laboratoires. 2018 Feb 1;2018(499):28–37.

40. Lee WH, Sonntag WE, Mitschelen M, Yan H, Lee YW. Irradiation induces regionally specific alterations in pro-inflammatory environments in rat brain. Int J Radiat Biol. 2010 Feb;86(2):132–44.

41. Lee JB, Kim MH, Chung YG, Park JY. Expression of cytokines in radiation injured brain at acute phase. Journal of Korean Neurosurgical Society. 2007 Sep 1;42:200–4.

42. XXXX et al. Cancer Radiother. 2024 Oct;28(5):474–83.

43. Zhou S, Huang Y, Chen Y, Liu Y, Xie L, You Y, et al. Reprogramming systemic and local immune function to empower immunotherapy against glioblastoma. Nat Commun. 2023 Jan 26;14(1):435.

44. Marcus D, Lieverse RIY, Klein C, Abdollahi A, Lambin P, Dubois LJ, et al. Charged Particle and Conventional Radiotherapy: Current Implications as Partner for Immunotherapy. Cancers (Basel). 2021 Mar 23;13(6):1468.

45. Laurent PA, Deutsch É. [Radiation-induced lymphopenia: Lymphocytes as a new organ at risk]. Cancer Radiother. 2023 Sep;27(6–7):511–8.

46. Damen PJJ, Lin SH, van Rossum PSN. Editorial: Updates on radiation-induced lymphopenia. Front Oncol. 2024 Jul 2;14:1448658.

47. Sadowski K, Jażdżewska A, Kozłowski J, Zacny A, Lorenc T, Olejarz W. Revolutionizing Glioblastoma Treatment: A Comprehensive Overview of Modern Therapeutic Approaches. Int J Mol Sci. 2024 May 26;25(11):5774.

48. Piotrowski, Anna F., Thomas R. Nirschl, Esteban Velarde, et al. 2018. Systemic Depletion of Lymphocytes Following Focal Radiation to the Brain in a Murine Model. OncoImmunology 7 (7): e1445951.

49. Sloan, Lindsey, Rupashree Sen, Chunnan Liu, et al. 2024. 'Radiation Immunodynamics in Patients with Glioblastoma Receiving Chemoradiation'. Frontiers in Immunology 15: 1438044.

50. Bergerud, Kyra M. Boorsma, Matthew Berkseth, Drew M. Pardoll, et al. 2024. 'Radiation Therapy and Myeloid-Derived Suppressor Cells: Breaking Down Their Cancerous Partnership'. International Journal of Radiation Oncology, Biology, Physics 119 (1): 42–55.

51. Kleinberg, Lawrence, Lindsey Sloan, Stuart Grossman, and Michael Lim. 2019. 'Radiotherapy, Lymphopenia, and Host Immune Capacity in Glioblastoma: A Potentially Actionable Toxicity Associated With Reduced Efficacy of Radiotherapy'. Neurosurgery 85 (4): 441–53.

Figure captions

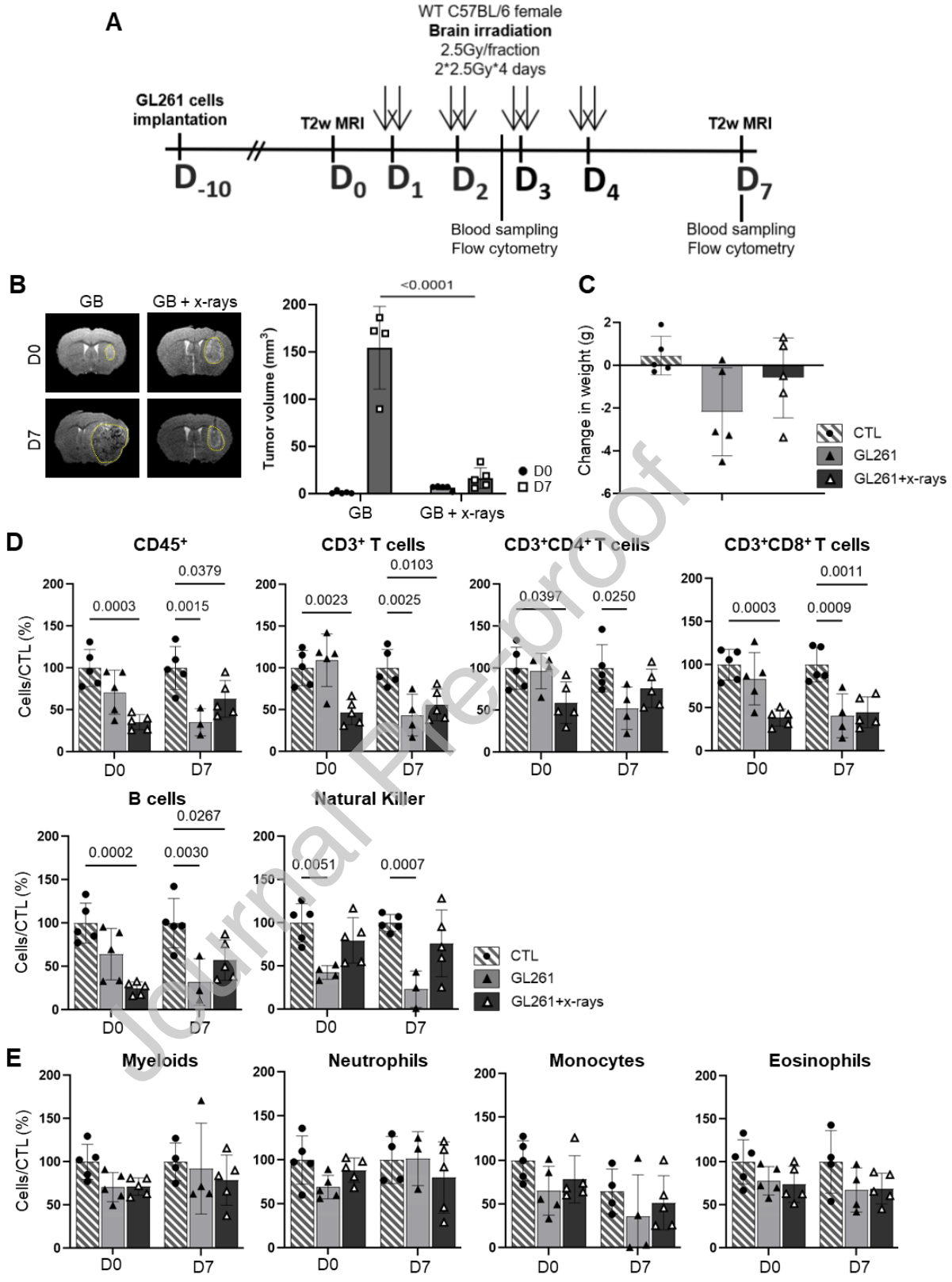

Figure 1. X-ray brain irradiation effects in GL261 tumor-bearing C57BL/6 mice. A. Experimental protocol. **B.** Tumor volume quantification before (D_0) or after (D_7) x-ray treatment in treated tumor-bearing mice (GL261+x-rays) compared with untreated tumor-bearing mice (GL261) (n=5 per group). **C.** Change in mice weight for treated tumor-bearing mice (GL261+x-rays) and untreated tumor-bearing mice (GL261) mice compared with CTL (n=5 per group). Mean ± standard deviation, one-way ANOVA along with a Tukey's multiple comparison test. **D-E.** Change in $CD45^+$ lymphoid (D) and $CD11b^+$ myeloid

(E) subtypes at D_2 and D_7 after x-ray brain irradiation (n=5 per group). Mean ± standard deviation, one-way ANOVA along with a Kruskall-Wallis multiple comparison test.

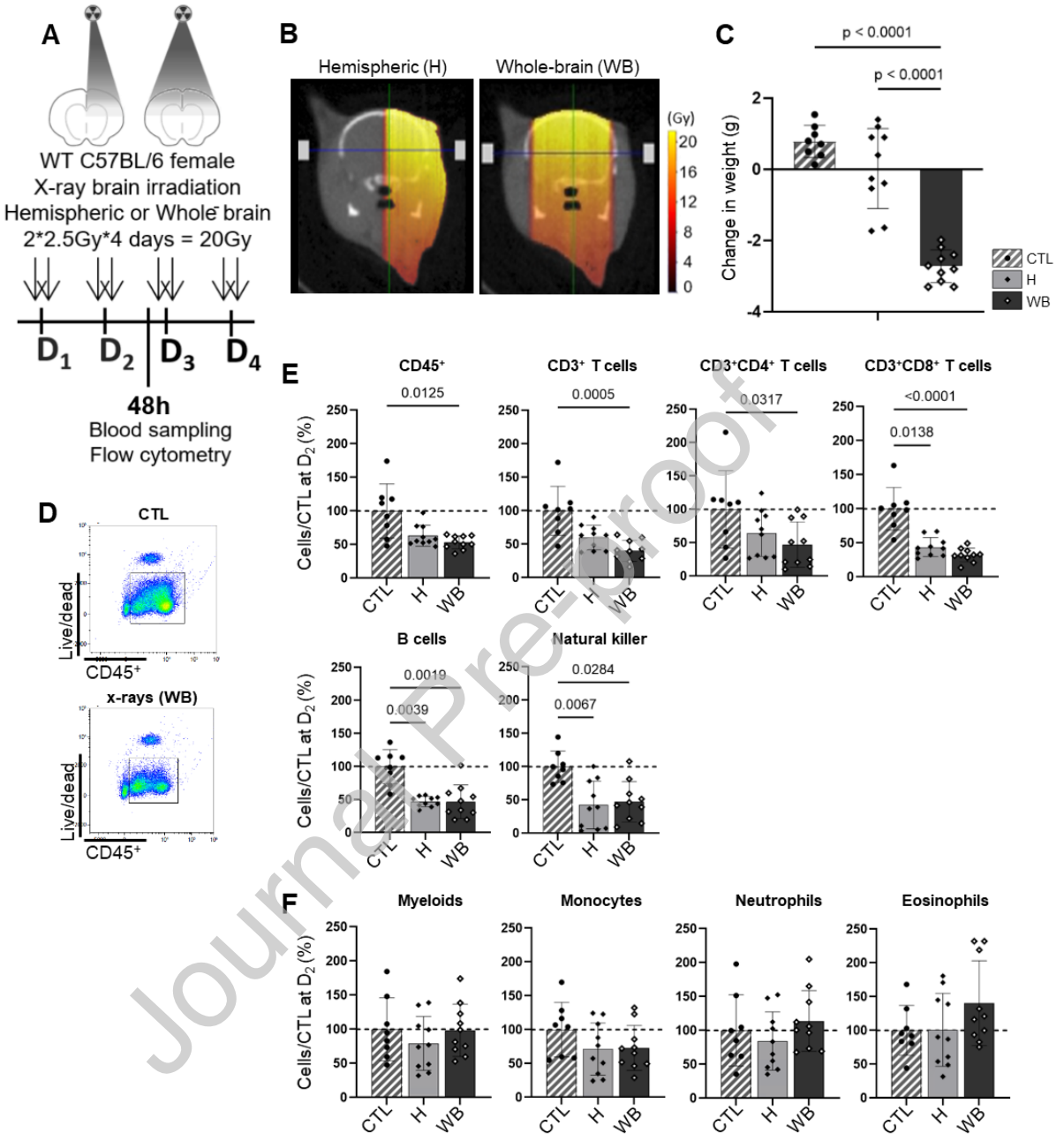

Figure 2. Change in lymphoid and myeloid populations after x-ray brain irradiation. A. Experimental protocol. **B.** Dosimetry maps representing x-ray hemispheric and whole-brain irradiation with a 20Gy dose. **C.** Change in weight after x-ray hemispheric (H) or whole-brain (WB) exposure (n=10) compared with controls (CTL) (n=8). Mean ± standard deviation, one-way ANOVA test with a Tukey's multiple comparison test. **D.** Dots plots illustrating the variation of CD45+ leucocytes cells at D2 after x-ray whole-brain (WB) irradiation compared with CTL. **E-F.** Change in CD45+ leucocytes and lymphocyte subtypes (E), and CD11b+ myeloid subtypes (F) after x-ray hemispheric (H) or whole-brain (WB) irradiation at D2 (n=10) compared with CTL (n=8). Mean ± standard deviation, one-way ANOVA test, along with a Kruskal-Wallis multiple comparison test.

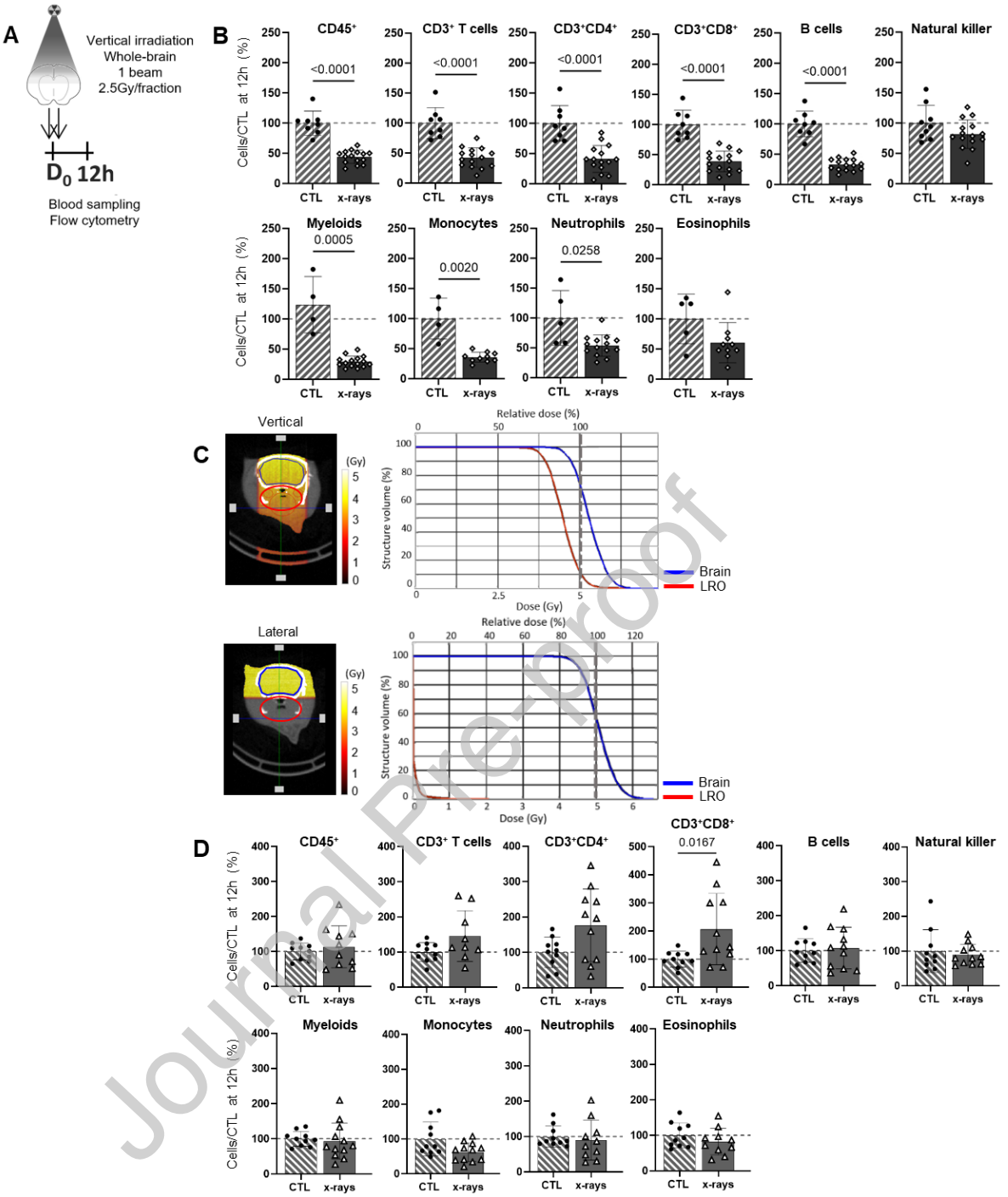

Figure 3. Change in lymphoid and myeloid populations after x-ray brain irradiation by challenging the onset time of lymphopenia and the beam orientation. A. Experimental protocol. **B-D.** Change in lymphoid and myeloid subtypes 12h after vertical (C) (irradiated, n=15; CTL, n=10) or lateral (E) (irradiated, n=10; CTL, n=10) x-ray brain irradiation compared with CTL. Mean ± standard deviation, Mann-Whitney test. **C.** Dosimetry maps representing the vertical and lateral x-ray whole-brain irradiation with a 5Gy dose and the associated dose-volume histogram illustrating the dose received for each structure of interest as a function of the dose set by the beam for the whole-brain vertical or lateral irradiation. LRO, lymphocyte-rich organs.

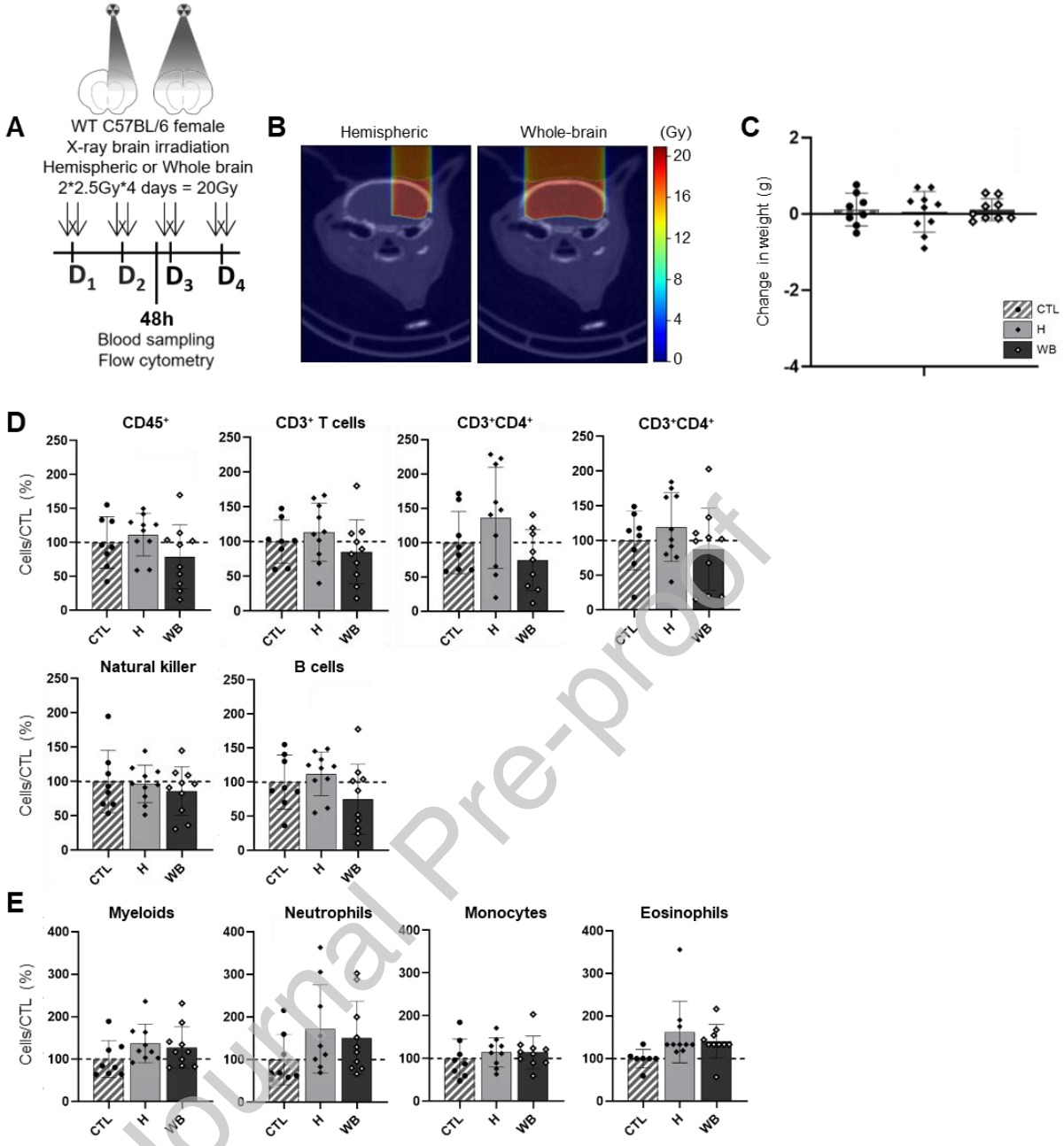

Figure 4. Change in lymphoid and myeloid populations after proton brain irradiation. A. Experimental protocol. **B.** Dosimetry maps representing proton hemispheric and whole-brain irradiation with a 20Gy dose. **C.** Change in weight after hemispheric (H) or whole-brain (WB) proton exposure (n=10) compared with controls (CTL) (n=8). Mean ± standard deviation, one-way ANOVA test with a Tukey's multiple comparison test. **D-E.** Change in CD45+ leucocytes and lymphocyte subtypes (D) and CD11b+ myeloid subtypes (E) after proton hemispheric (H) or whole-brain (WB) irradiation (n=10) at D2 compared with CTL (n=8). Mean ± standard deviation, one-way ANOVA test, along with a Kruskal-Wallis multiple comparison test.

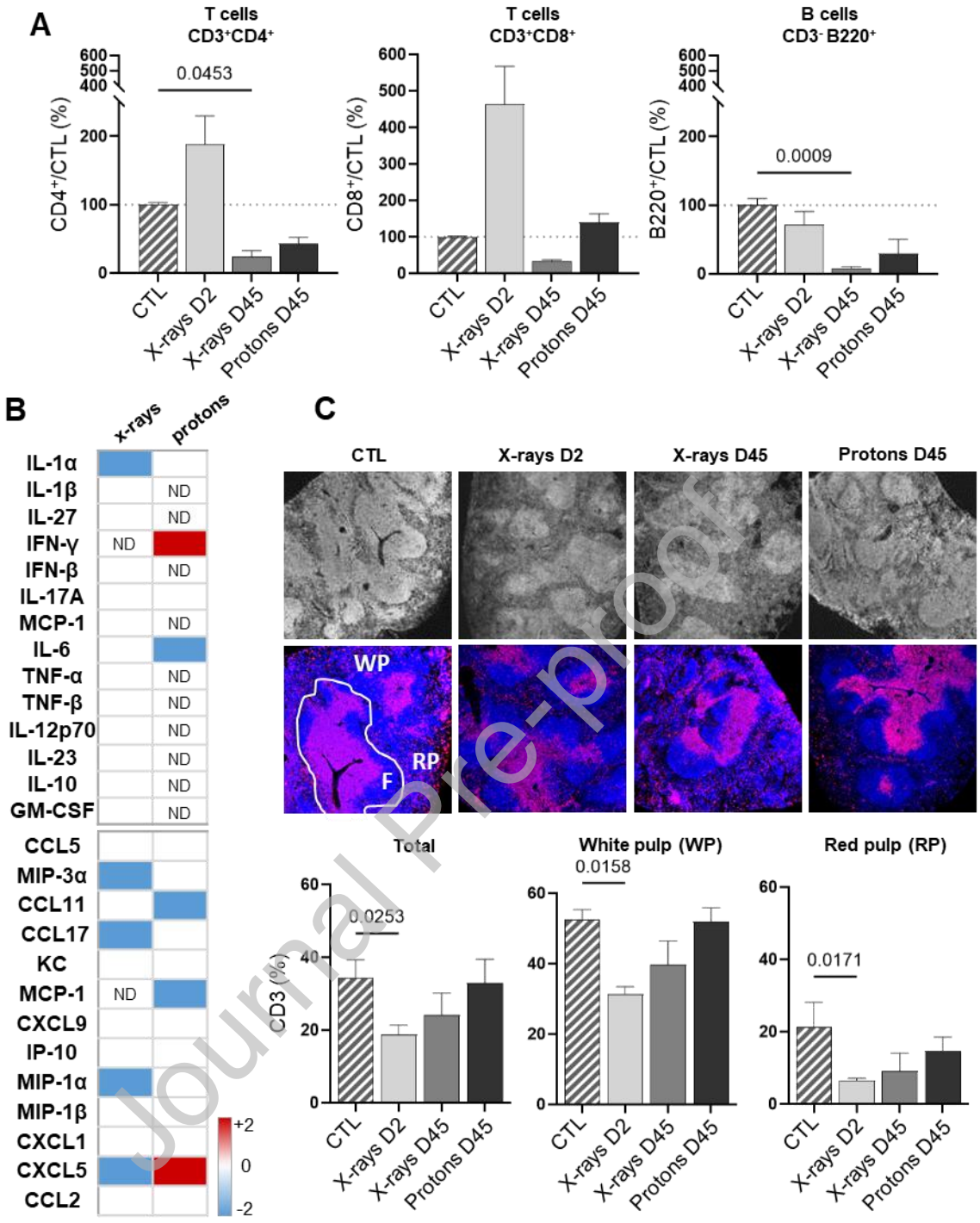

Figure 5. Crosstalk between brain irradiation, the circulating compartment and the secondary lymphoid organs. A. Quantification of CLN lymphocyte subpopulations by flow cytometry after x-ray (D2 and D45) or proton (D45) brain irradiation. Mean ± standard deviation, one-way ANOVA along with a Kruskal-Wallis multiple comparison test (n=5 per group). **B.** Change in cytokines in the plasma of x-ray or proton brain irradiated mice (n=10 per group). Data were expressed as the percentage expression relative to control (n=8). Some row values were below the normal detection threshold, therefore 'not detected' (ND). **C.** Representative CD3 (red) and Hoechst 33342 (blue) fluorescence in the spleen after x-ray (24h and D45) or proton (D45) brain irradiation. Up = x5. Down = x10. F, follicle. RP, red pulp. WP, white pulp. Mean ± standard deviation, one-way ANOVA test, along with a Kruskal-Wallis multiple comparison test (n=4 per group).